46. J. S. Lyon, T. J. Hilliard, T. N. Bethell, *The Burden of Gilt* (Mineral Policy Center, Washington, DC, 1993).
47. *McLaughlin Mine: General Information Summary* (Homestake Mining, San Francisco, 1990).
48. R. E. Krauss, seminar lecture, Stanford University (20 May 1992).
49. "Kennecott Smelter to Be Cleanest," *Min. J.* **321**, 382 (1993).
50. A. Warhurst, *Nat. Resour. Forum* **16**, 39 (1992).
51. ———, in (*42*), p. 133.
52. M. A. von Below, *Resour. Policy* **19**, 177 (1993).
53. *Min. J.* **317** (Environ. Suppl.) (1991).
54. R. Auty and A. Warhurst, *Resour. Policy* **19**, 14 (1993).
55. *ICME Newsl.* **1**, 4 (1993). Within the International Council on Metals and the Environment environmental charter are mandates to assign high corporate priority to environmental management and integration of environmental policies, programs, and practices, to consider ecological and cultural values along with economic benefits of development, and to support research on and promote the international transfer of technologies that mitigate adverse environmental effects.
56. A. Warhurst, *Newsl. 3* (Mining and Environment Research Network, Brighton, UK, 1992).
57. W. K. Reilly, Second Payne Lecture, Institute for International Studies, Stanford University (12 January 1994). Reilly maintained that public opinion in the industrial world has come down overwhelmingly in support of environmental protection, a fact corporations can expect to see reflected in consumer demand.
58. United Nations Department of Economic and Social Development (UNDESD) and Government of Zimbabwe, "Interregional Seminar on Guidelines for the Development of Small/Medium Scale Mining," Harare, Zimbabwe, 15 to 19 February 1993 (United Nations, New York, March 1993).
59. *The World Bank and the Environment, Fiscal 1993* (World Bank, Washington, DC, 1993).
60. T. L. Friedman, *New York Times* (24 July 1994), p. 8(N).
61. *Development, Environment and Mining: Post-Conference Summary* (International Council on Metals and the Environment, Washington, DC, June 1994).
62. "PNG Tries to Calm Investor's Fears as OK Tedi Fares Crisis," *Platt's Met. Week* **65**, 5 (23 May 1994).
63. "Newmont Gold's Indonesian Milestone," *Min. J.* **323**, 127 (1994).
64. G. E. Lagos, in (*42*), p. 85.
65. N. Myers, *Ultimate Security: The Environmental Basis of Political Stability* (Norton, New York, 1993).
66. O. Bomsel, in (*67*), p. 59.
67. J. E. Tilton, Ed., *Mineral Wealth and Economic Development* (Resources for the Future, Washington, DC, 1992).
68. "Zambia Adrift," *Min. J.* **322**, 295 (1994).
69. P. Daniel, in (*67*), p. 81.
70. "The Mining Industry in 1993," *Min. J.* **321**, 440 (1993).
71. *Development and the Environment: World Development Report 1992* (Executive Summary, World Bank, Washington, DC, 1992).
72. Zaire had a total of 12 million people in 1950; in 1995, it will have 44 million, and by 2025, likely more than 104 million. Between 1950 and 2025, Zambia's population will have grown from 2.4 million to about 21 million. In moderately developed South Africa, population more than tripled in 45 years, from 13.7 million in 1950 to an estimated 43 million in 1995, with 73 million projected by 2025 (*13*).
73. O. Bomsel and C. von Hirschhausen, presented at the Second Annual Professional Meeting of the Mineral Economics and Management Society, Reno, NV, 18 to 20 February 1993, p. 187.
74. *Min. J.* **320** (suppl.), 185 (1993).
75. *ibid.* **322**, 142 (1994).
76. "Pollution Fine for Norilsk Nickel Combine," *ibid.* **320**, 159 (1993); "Norilsk Privatization Lures Russian Private Investors," *Platt's Met. Week* **65**, 5 (20 June 1994).
77. "Mexico: New Investment Law," *Min. J.* **322**, 23 (1994).
78. O. Martino, J. Machamer, I. Torres, *The Mineral Economy of Mexico* (U.S. Bureau of Mines, Washington, DC, 1992).
79. "Mining Industry Takes a Look at NAFTA," *Met. Week* **63**, 7 (21 September 1992).
80. W. P. Blacutt-Mercado, *Nat. Resour. Forum* **17**, 207 (1993).
81. "Bolivia Privatizing Quickly," *Platt's Met. Week* **65**, 5 (9 May 1994).
82. World Bank, Mining Unit, Industry and Energy Division, *Strategy for African Mining* (World Bank, Washington, DC, 1992).
83. O. Bomsel, *The Future of Mining Countries: New Strategies or the Restructuring of the State?*, prepared for United Nations Conference on Trade and Development (1994).
84. G. A. Morgan, *The Mineral Economy of Guinea* (U.S. Bureau of Mines, Washington, DC,1992).
85. "Liberian Iron Ore Mining to Resume," *Min. J.* **322**, 102 (1994).
86. K. Horta, presented at the meeting of the World Heritage Committee, Cartagena, Colombia, 7 December 1993.
87. *Economic Implications of A Royalty System for Hardrock Minerals* (U.S. Department of the Interior, Washington, DC, 1993).
88. I thank numerous colleagues for provocative discussions, particularly E. A. Thiers, J. J. Schanz, M. C. Frippel, G. Nash, W. P. Blacutt, and S. Strauss, all of whom offered valuable commentary. Formal reviewers S. D. Ludington, J. J. Rytuba, and E. A. Thiers were particularly helpful in their suggestions for improving the manuscript, as were H. R. Spall and B. R. Lipin. Comments by B. J. Skinner, C. Brandon, A. Cendrero, and two anonymous reviewers were most beneficial. K. Horta provided information regarding the Mount Nimba project. S. Garcia crafted the illustrations. The basic concept of this paper is a product of my year's affiliation (1992) with Stanford University, where I developed a course on "Minerals and World Affairs" as a visiting professor in the School of Earth Sciences, under the National Science Foundation's Visiting Professorships for Women program. I thank the U.S. Geological Survey for permitting me to continue this research.

RESEARCH ARTICLE

Mutagenesis and Laue Structures of Enzyme Intermediates: Isocitrate Dehydrogenase

Jill M. Bolduc, David H. Dyer, William G. Scott, Paul Singer, Robert M. Sweet, Daniel E. Koshland Jr., Barry L. Stoddard*

Site-directed mutagenesis and Laue diffraction data to 2.5 Å resolution were used to solve the structures of two sequential intermediates formed during the catalytic actions of isocitrate dehydrogenase. Both intermediates are distinct from the enzyme-substrate and enzyme-product complexes. Mutation of key catalytic residues changed the rate determining steps so that protein and substrate intermediates within the overall reaction pathway could be visualized.

Standard x-ray crystallography is usually performed on inactivated enzymes or inhibited enzyme complexes in order to prevent the rapid reaction of substrate and time-dependent averaging of electron density. However, polychromatic Laue crystallography, a technique whereby the x-ray source is a synchrotron, provides an increased rate for data collection so that the structural details of intermediate complexes can be visualized (*1–5*). Such Laue studies demonstrate the possibility of visualizing rate-limited enzyme-substrate complexes with very long lifetimes, but do not address the problem of transient intermediate species that normally are not rate-limited.

Determination of the structure of an enzyme-bound intermediate on a path of several intermediates requires a method of inducing the homogeneous synchronized accumulation of that particular species throughout the crystal, during which time diffraction data may be collected. One successful strategy has consisted of triggering an initial, synchronized turnover cycle in the crystal with a caged-type compound (usually a chemically modified substrate molecule that can be released by flash photolysis). During the first round of catalysis after photolysis, rate-limited intermediates accumulate and then decay, provided that the rate of all steps between the initial absorption of photons and the formation of the rate-limited intermediate complex are sufficiently fast. As an alternative strategy we now present the use of site-directed mutagenesis of key catalytic residues to create kinetic bottlenecks at specific catalytic steps in the overall reaction pathway that may then be used to determine the structure of distinct intermediates. Such complexes represent steady-state species that accumulate and persist in the crystal in vast excess of other catalytic states during the course of slow turnover and data collection.

The use of slow catalytic enzyme mutants to elucidate the structure of intermediate states during time-resolved crystallographic experiments has been suggested (*6–8*) and exploited (*9–11*), but such mutants have customarily been applied to nonproductive, dead-end enzymatic complexes rather than intermediates on an active catalytic pathway. However, this technique makes it possible to visualize the structure of transient intermediates that do not normally accumulate during turnover. If a mutant enzyme displays the same chemical mechanism as the wild-type catalyst, but with an extreme rate limit at a single reaction step, then this complex may be examined by means of fast diffraction techniques.

The enzyme chosen for this approach, isocitrate dehydrogenase (IDH), performs the reaction shown in Eq. 1. The enzyme follows a random binding mechanism and forms initial binary substrate complexes (complexes 2 and 3 in Eq. 1) that then proceed to an ordered ternary Michaelis complex (step 4). Dehydrogenation of isocitrate produces the putative intermediate oxalosuccinate (OSA, step 5) that then undergoes an elimination of its β carboxyl to generate α-ketoglutarate (step 6). The binary substrate complexes have been previously visualized using monochromatic x-ray crystallography (*12, 13*). The intermediate oxalosuccinate has been postulated (*14*) and supported by isotopic experiments (*15*), but isolation from a reaction starting with reactants or products has not materialized; it was presumed to be generated transiently and decompose faster than it dissociated. Oxalosuccinate has been added to the enzyme and shown to give isocitrate (the reverse reaction) or α-ketoglutarate (the forward reaction) but at rates that are not as fast as the overall reaction (*16*). This difference is probably due to a slower rate of binding for the intermediate species than for the natural substrates of the overall reaction. Amino acid mutagenesis together with x-ray data have provided support for the amino acid residues Tyr^{160} and Lys^{230} as key catalytic residues on the reaction pathway (*12, 16*). Mutagenesis of these two residues decreased the rate of dehydrogenation (k_{dehyd}) and elimination (k_{elim}), respectively, allowing the visualization of complexes 4 and 5 in Eq. 1.

J. M. Bolduc, D. H. Dyer, and B. L. Stoddard are at the Fred Hutchinson Cancer Research Center, Program in Structural Biology, Division of Basic Sciences, 1124 Columbia Street A3-023 Seattle, WA 98104. W. G. Scott is at the Molecular Research Council, Laboratory of Molecular Biology, Hills Road, Cambridge England CB2 2QH. P. Singer and R. M. Sweet are at the Brookhaven National Laboratories, Department of Structural Biology, Upton, Long Island, NY 11973. D. E. Koshland Jr. is in the Department of Molecular and Cell Biology, Stanley Hall, University of California, Berkeley, CA 94720.

*To whom correspondence should be addressed.

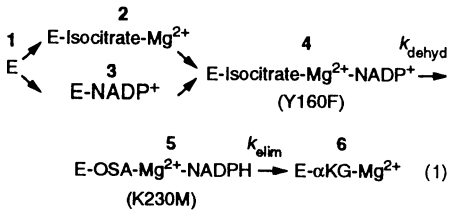

We therefore used the two mutants (i) Y160F, in which Tyr^{160} was converted to Phe, and (ii) K230M, in which Lys^{230} was converted to methionine, to accumulate specific intermediates in the crystal and create bottlenecks in the enzymatic reaction. The evidence that the mutants follow the same chemical mechanism as the wild-type enzyme is (i) the mutagenized proteins have the same structure as wild-type enzyme, (ii) they bind substrate at the active site in a conformation and position identical to wild-type enzyme, (iii) they exhibit the same $NADP^+$-dependent process of dehydrogenation as the wild-type enzyme, and (iv) although for each mutant a particular step in the reaction pathway is slowed by the localized mutagenesis, their remaining individual catalytic steps proceed at rates comparable to those of the wild-type enzyme (*16*).

Steady-state structure determination of rate-limited species for isocitrate dehydrogenase. Polychromatic x-ray diffraction data were collected first from several crystals of each mutant before continuous presentation of saturating substrate with a flow cell and then at two specific times after accumulation of the steady-state complex while continuing to apply substrate. Data were collected at beamline X-26C at the

Table 1. Diffraction data statistics. Steady-state Laue studies were performed on both site-directed mutants of the enzyme isocitrate dehydrogenase using multiple crystals of approximately the same dimensions (0.3 to 0.5 mm on each side). The space group and unit cell dimensions in all cases were $P4_32_12$, with $A = B$, 105 Å; $C = 150$ Å. The diffraction data were obtained with Fuji imaging plates at beamline X26-C (Brookhaven National Laboratories) and scanned with a BAS-2000 phosphor image plate reader; and subsequent refinement was done by means of X-PLOR (*18*). For both sets of experiments, 75 ms exposures before presentation of substrate (at $t = 0$ seconds) were followed by saturation of the crystals with 500 mM substrates (isocitrate, Mg^{2+}, $NADP^+$ in 35 percent saturated ammonium sulfate, pH 7.0) with a flow cell. Identical exposures of the resulting steady-state enzyme complexes were then collected at 60 and 360 seconds. For each mutant, the same experiment was repeated with four crystals in arbitrary orientations, and the data collection at the same time points, so that the R_{merge} (on intensities I) represents data from four separate crystals at that time point. The merged data from separate time points for each mutant were used to calculate overall isomorphous differences (R_{iso}) between time points, prior to calculation of difference maps. The overall isomorphous difference in structure factor amplitudes (F_s) between data collected before and after substrate binding are 13 to 15 percent, or about 30 percent on intensities. These differences decrease when data collected at 60 and 360 seconds are compared, an indication that the crystals are fully saturated. The structure factor intensities were integrated and merged according to standard Laue processing packages (*23*). The program LAUEGEN produces and refines an orientation matrix based on vector matching between the obvious harmonic overlaps on each image. The reflections were then integrated by means of the program INTLAUE. Harmonic overlaps (which represent most of the low-resolution terms) were discarded. The data from the same time points of the experiment (but from different crystals) were then merged, scaled, and normalized against wavelength (with the use of symmetry-related reflections) with the program LAUENORM.

Mutant	Time (s)	Crystals	R_{merge}*	Redundancy†	Completeness (%)‡ 100–2.5 Å	Completeness (%)‡ 4–2.5 Å	I/σ (I) (avg)	R_{iso} (vs t = 5 minutes)§
Crystal to crystal merging								
Y160F	0	4	0.082	17.3	67	83	19.4	0.126
Y160F	60	4	0.084	17.3	66	82	22.3	0.045
Y160F	360	4	0.093	17.3	65	84	21.5	. . .
K230M	0	4	0.092	18.7	62	80	19.1	0.138
K230M	60	4	0.089	18.7	62	82	16.6	0.037
K230M	360	4	0.098	18.7	61	81	25.4	. . .

	Y160F		K230M	
	Apo	Steady state	Apo	Steady state
Final refinement statistics (10 to 2.5 Å resolution)				
Unique structure factors	17933	17943	17204	17316
R_{refine}‖	0.183	0.172	0.174	0.169
rmsd bond distance (Å)	0.017	0.019	0.019	0.018
rmsd bond angles (°)	3.58	3.79	3.49	3.66
rmsd dihedral angles (°)	25.1	26.2	24.5	25.1
rmsd impropers (°)	2.5	2.2	2.3	1.8

*$R_{merge} = \Sigma_j (I_1 (j) - I_2 (j)) / \Sigma_j (I (j))$; †Redundancy = ratio of total measured reflections to total unique reflections in final data set; ‡Completeness = ratio of measured unique reflections to the number of predicted unique reflections; §$R_{iso} = [(\Sigma | |F_{P1}| - |F_{P2}| |) / \Sigma (|F_{P1}|)]$; ‖$R_{refine} = [\Sigma j | (F_o (j) - F_c (j)) | / \Sigma_j (F_o (j))]$. The final refinement statistics for steady-state complexes are for $t = 60$ seconds.

Brookhaven National Synchrotron Light Source (*17*) (Table 1). We used multiple crystals for each mutant (rather than collecting several exposures from the same crystal in different orientations before and after substrate binding) because these crystals do not physically survive an extended presentation of substrate and slow turnover in addition to multiple polychromatic x-ray exposures. In order to examine through difference maps whether a true steady state would be formed by the first time point as indicated by spectroscopic diffusion studies, we collected data at discrete time points with multiple crystals so that we could examine this question in addition to determining the structure of the complexes.

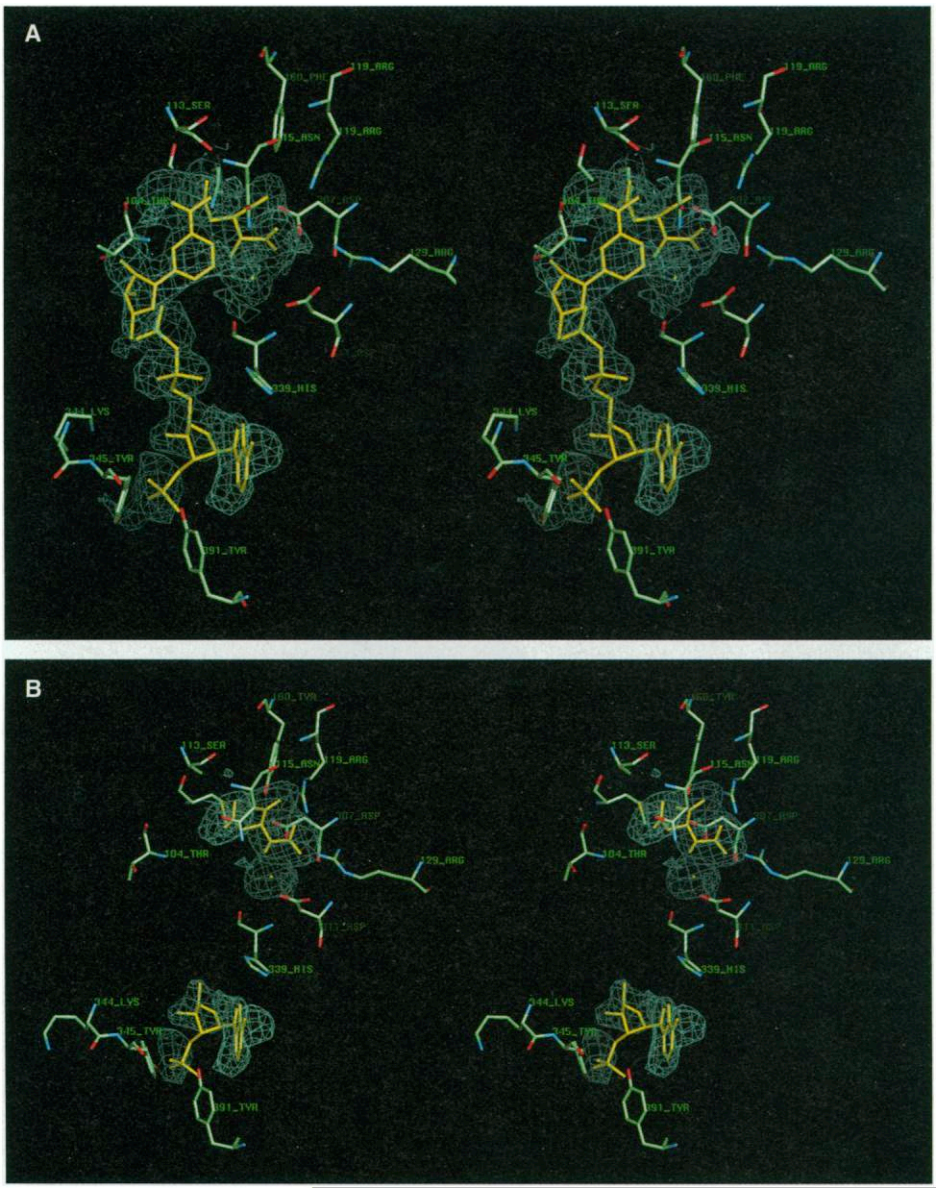

Fig. 1. Crystallographic structure of the rate-limited substrate-enzyme complexes for isocitrate dehydrogenase [(**A**) Y160F; and (**B**) K230M] at 2.5 Å resolution. These two difference maps indicate rate-limited complexes that correspond to species 4 and 5, respectively, in Eq. 1. Experimental difference maps of the active sites of both kinetic mutants were calculated with Fourier coefficients [F_o (60 seconds after substrate) − F_o (before substrate presentation)] α_{calc}. Phases were back-calculated for each map with the use of previously determined atomic coordinates for the apo form of each mutant. Difference maps were calculated (i) before initial refinement of the protein model against the measured data, and (ii) after initial refinement with the protein model only (as shown). Both sets of maps clearly indicate the presence of well-occupied, productive substrate complexes that accumulate as a result of the kinetic rate barriers at specific catalytic steps. The initial *R* factors for the protein model before refinement were approximately 30 percent; the *R* factor after initial refinement with protein coordinates only (leading to the difference maps shown) were both approximately 22 percent. The refined thermal *B* factors for the substrate models average between 20 and 30 Å^2 and are in agreement with the surrounding protein side chains. These maps are contoured at 3 σ; the features shown are the strongest ones over the entire enzyme molecule. All modeling and figure preparation was carried out on a Silicon Graphics XS-24 workstation with the software QUANTA (Molecular Simulations, Inc.).

For calculating difference maps (Fig. 1) we used phases from protein coordinates before refinement and then again after an initial round of refinement against the Laue data with X-PLOR (*18*). No substrate or water molecules were included in either phase calculation. The strongest features of the maps were easily modeled by the rate-limited enzyme complexes. Although the data are less complete than typical monochromatic data sets (82 percent between 4 Å and 2.5 Å resolution, but much less complete coverage at lower resolution), the difference maps are of high quality because of high data redundancy (almost 20-fold for both data sets), low background, and high occupancy complexes. Recent studies (*5*) indicate that high quality difference maps are possible at similar resolution (2.2 Å) from even less complete polychromatic data recorded on x-ray film when processed accurately with the appropriate polychromatic data reduction software. Additional difference maps calculated from differences between the data collected 60 seconds in comparison to 5 minutes after substrate binding are featureless, indicating formation of a true steady state. This result agrees with the low isomorphous differences between these time points (Table 1), and indicates complete binding and saturation consistent with the results of spectroscopic monitoring of diffusion in the crystal described below.

Visualization of the rate-limited ternary Michaelis complex (Y160F). Kinetic experiments (see below) show that Y160F exhibits a large reduction in the rate of hydride transfer from isocitrate and also show that there is no difference in apparent binding constants and on-rates, or in the rate of the decarboxylation step that directly follows the hydride transfer. A high percentage of the enzyme active sites in the crystal accumulate this productive complex during continuous saturation of the crystal with high concentrations of the substrates. The electron density from difference Fourier maps can be modeled by $NADP^+$ and isocitrate-Mg^{2+} by means of simple adjustments in torsion angles through the pyrophosphate backbone (Fig. 1A). The crystallographic electron density for the adenosyl portion of the cofactor and for the bound isocitrate molecule agree with that for previously solved binary complexes of IDH (*12*, *13*). The peak corresponding to the bound magnesium ion (the largest feature of the map at 12-sigma contour levels) indicates bond lengths to isocitrate of 2.2 to 2.4 Å.

Isocitrate is closely associated with the *re* face of the sp^2 prochiral C4 carbon of the nicotinamide ring, as expected for an A-type dehydrogenase such as IDH (*19*). This

alignment allows hydride transfer from the C2 carbon of the substrate to C4 of the nicotinamide ring, with stereospecific incorporation of a hydrogen at that position. The distance from the hydride donor to acceptor is 3.0 Å, and the angle through the planar nicotinamide ring to the substrate hydride donor carbon is 110°. This distance and the angle are consistent with other previously solved dehydrogenase ternary complexes, whose bond distances range from 2.3 to 3.9 Å and 101° to 147°, respectively (*20*). Isocitrate moves by approximately 0.5 Å toward the nicotinamide ring as compared to the binary complex of isocitrate and Mg^{2+}. This motion appears to occur primarily as a rigid body, with the contacts between protein side chains and the carboxylates of isocitrate being maintained in the ternary complex. A rotation of the bond between C4 and C5 of isocitrate of approximately 15° frees the γ carboxyl of the substrate from a steric overlap with the nicotinamide ring and, at the same time, maintains a hydrogen-bond interaction with the γ oxygen of Ser^{113}. The close association of substrate, the nicotinamide nitrogen, and Ser^{113} is consistent with the kinetic effects of site-specific mutations at that position (*21*).

The $NADP^+$ cofactor is bound in an extended conformation with a distance of 14 Å between the centers of the adenosyl and nicotinamide rings. The phosphate backbone passes approximately 5 Å from the bound metal, and leads into well-ordered density for the ribose and nicotinamide rings. The ribose ring displays a C4′ *endo* pucker, which acts to allow proper orientation of the nicotinamide ring relative to the substrate molecule. The interactions of the nicotinamide group appear to be primarily to the bound substrate, through polar interactions between the γ carboxyl of isocitrate and the nicotinamide ring nitrogen and amide group.

A pair of interactions between the cofactor and the enzyme appear to play a role in positioning the nicotinamide ring properly and in activating its C4 carbon for electrophilic substitution, thereby lowering the transition state energy during dehydration. These contacts represent the most significant protein dynamic movements when the Michaelis complex is formed. The side chain of Thr^{104} moves by 2.5 Å to form a hydrogen bond to the 2′ hydroxyl oxygen of the nicotinamide ribose. The distance between oxygens in the complex is 2.7 Å. This movement appears to stabilize the sugar in the configuration necessary to bring the nicotinamide C4 carbon within distance for the hydride transfer. In addition, Asn^{115} moves by 1.0 Å to make a 2.9 Å contact with the *si* face of the cofactor at the sp^2 chiral C4 carbon. The interaction is directly on the opposite side of the nicotinamide ring from the isocitrate molecule. The effect of the interaction between the asparagine amide nitrogen and the C4 hydrogen might be to activate the site for electrophilic attack and hydride transfer. This would be in agreement with the lowering of V_{max} and K_m for $NADP^+$ cofactor by mutating the residue to Asp or Leu. Apart from the residue movements described above, the structure of the protein backbone is virtually identical to that of the free enzyme, with a root-mean-square (rms) difference of 0.2 Å along the backbone, and 0.5 Å for all atoms, implying that these motions of well-ordered active site residues are significant, and that they do not represent fluctuations produced by refinement.

This structure is analogous to the previously described ternary complex of enzyme, isocitrate, $NADP^+$, and calcium (*22*), where Ca^{2+} was substituted for Mg^{2+} to produce a nonproductive enzyme complex. However there are substantial differences between the structure of that dead-end complex and the productive, slow mutant described now. Most important, the metal-substrate bond distances are much shorter for the productive complex, and the nicotinamide ring and ribose ring are bound in a different conformation and with interactions to the enzyme active site side chains that facilitate hydride transfer and catalysis.

Visualization of the subsequent oxalosuccinate complex (K230M). The lysine-to-methionine mutation at residue 230 causes a severe decrease in the rate of enzymatic decarboxylation of oxalosuccinate, but a much smaller reduction in the preceding rate of hydride transfer, which, in turn,

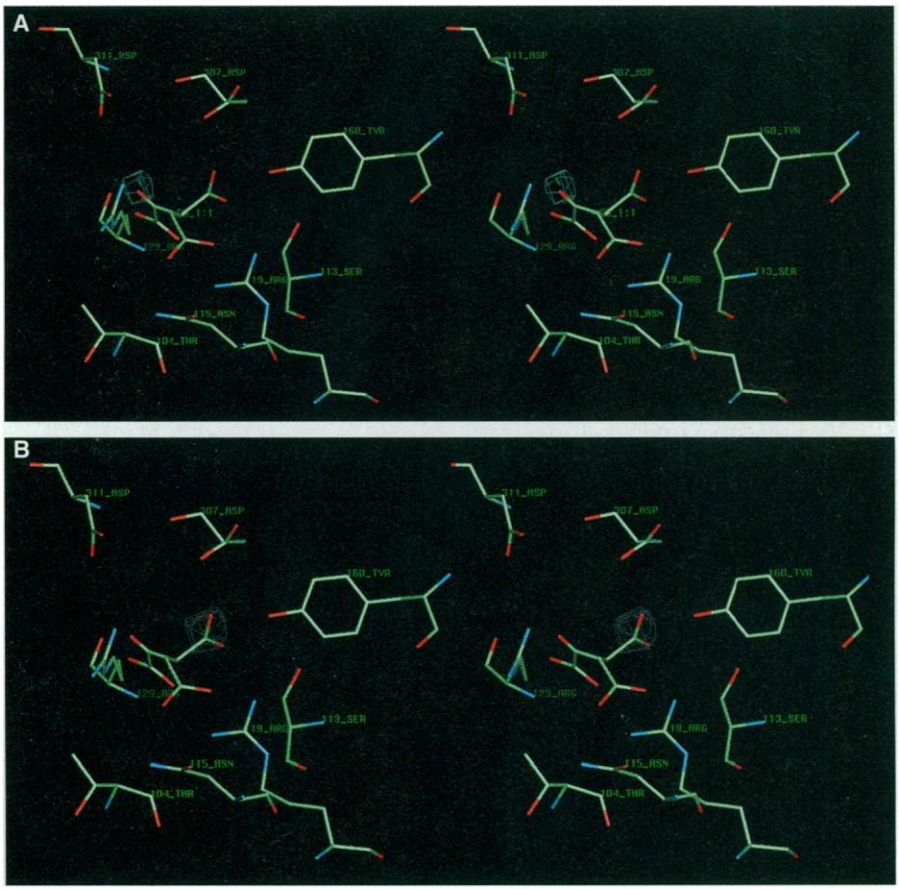

Fig. 2. Calculated difference maps for the mutant K230M at the site of the bound substrate-intermediate indicate the accumulation of oxalosuccinate in excess of either isocitrate or α-ketoglutarate. Maps were generated with Fourier coefficients F_o (K230M rate-limited complex) − F_c (calculated using the coordinates of either isocitrate of α-ketoglutarate ± CO_2 from a pair of test refinements against this data set with these compounds) in order to directly examine differences in electron density between the observed complex and the structure of the substrate or product of the reaction. A single overall *B* factor was refined for each substrate or product model. As shown in (**A**), difference maps calculated when isocitrate is used as the refinement model show a weak difference peak at the C2 carbon and hydroxyl oxygen, corresponding to the spectrophotometrically observed hydride transfer and accumulation of reduced NADPH for this mutant. Difference maps against α-ketoglutarate (**B**) without a covalently bound CO_2 at the C3 carbon indicate a strong feature of positive density at that position, implying the presence of oxalosuccinate rather than the final α-ketoglutarate product of the rate-limited decarboxylation for this mutant.

results in the accumulation of an intermediate complex of oxalosuccinate, Mg^{2+}, and reduced cofactor (NADPH) in the crystal. Thus, a similar experiment to that performed for the Y160F mutant allows visualization of an intermediate in which oxalosuccinate is clearly discerned.

The structure of the steady-state, rate-limited substrate complex in the K230M mutant (Fig. 1B) differs from similar maps calculated for Y160F, indicating that the predominant rate-limited catalytic state for K230M is distinct from that observed for Y160F, in agreement as judged from rate studies and single-crystal microspectroscopy. Difference maps show strong density corresponding to bound substrate and magnesium, as well as density for the adenosyl ring and adjoining ribose sugar of the NADP(H) cofactor. The crystallographic electron density for the adenosyl portion of the cofactor and for the bound oxalosuccinate molecule agree with the positions observed in binary complex structures (*12*, *13*). However, the nicotinamide ring and phosphate backbone of NADPH are disordered, a result that is similar to the bound structure of $NADP^+$ in the absence of substrate and metal. The absence of electron density for the nicotinamide ring in the K230M structure is probably caused by the loss of strong attractive electrostatic forces between the substrate carboxylates and an uncharged NADPH, as compared to the complex of isocitrate and $NADP^+$.

In order to confirm the assignment of the observed rate-limited catalytic species in this experiment as oxalosuccinate, F_o-F_c difference Fourier maps were calculated for the bound complex after refinement with the catalytic species which directly precede and follow oxalosuccinate on the reaction pathway (isocitrate and α-ketoglutarate + CO_2, respectively), as shown in Fig. 2. These maps reveal (i) difference peaks at the C2 carbon and hydroxyl oxygen relative to isocitrate, consistent with the loss of a hydride and formation of an sp^2 carboxyl group, and (ii) a covalently bound β carboxyl at the C3 carbon relative to α-ketoglutarate, indicating that the rate-limited intermediate has not proceeded through the elimination reaction to yield α-ketoglutarate and free CO_2. This agrees with the kinetic profile of the K230M mutant as discussed below.

Oxalosuccinate and magnesium are shifted by approximately 0.5 Å away from Ser^{113} and toward the conserved Asp^{311} and Asp^{307}, which bind the transition metal. The hydrogen bond between the γ carboxylate of oxalosuccinate and the Ser 113 hydroxyl is maintained, partly by a movement of the serine side chain and backbone by just less than 1 Å. The distance from the oxalosuccinate C2 carboxyl oxygen and the C1 carboxyl oxygen to the bound calcium is 2.3 Å. In the resulting complex, the mutated side chain at residue 230 is still oriented to facilitate elimination of the β carboxyl, but with a distance of approximately 4 Å from the unreactive terminal methylene carbon of the methionine side chain to the substrate, as opposed to the 2.6 Å distance from the lysine amino group to the substrate carbonyls seen in the wild-type binary complex (*12*). The largest protein movement in the active site is the return of Thr^{104} and Asn^{115} to their original positions in the uncomplexed state. This movement corresponds to the release of the nicotinamide ring and ribose from well-ordered bound positions after hydride transfer.

Consistency with kinetic studies. For solving the structure of a rate-limited intermediate by means of Laue crystallography

Table 2. Rate constants in solution were determined as described (*16*, *20*). Potassium oxalosuccinate (OSA) was prepared (*24*), and the concentrations of α-ketoglutarate and OSA were determined (*15*). The rates of dehydrogenation of isocitrate (k_{dehyd}) in the presence of NADP were measured by monitoring the change in absorbance at 340 nm. The rate k_{dehyd} was measured as an initial kinetic burst by stopped-flow spectroscopy; the rate for Y160F k_{dehyd} is assumed to be equivalent to the overall forward rate, in that no burst is observed under these conditions. The reverse rate of reduction of oxalosuccinate (k_{hyd}) were measured in a similar fashion by measuring the disappearance of NADPH at 340 nm. The decarboxylation of oxalosuccinate (k_{elim}) was measured spectrophotometrically at 240 nm. The overall forward rate constant exceeds the measured rate of conversion of oxalosuccinate to α-ketoglutarate (when oxalosuccinate is used directly as a substrate in the assay) for wild-type enzyme and K230M because of a slower on-rate for the intermediate than for the natural substrates of the overall reaction. Therefore, rate studies with oxalosuccinate provide a relative comparison of individual rate-barriers for separate enzyme species, but do not indicate the absolute rate of this step when isocitrate is bound and converted to α-ketoglutarate. Rate constants in the crystal were measured spectrophotometrically as described in Fig. 3, by mounting individual crystals in flow cells, applying varying substrate concentrations to the crystals, and monitoring the production of product in the effluent on a spectrophotometer with a dead-end continuous-flow cuvette (NSG Precision Cells). Overall initial steady-state kinetics may be measured in the crystal, but not individual rate constants. Calculation of the rate of product production from the enzyme crystal, compared to the number of molecules measured to populate the internal volume of the crystal demonstrate that the entire population is catalytically active (Fig. 3).

Kinetic constant	Enzyme species					
	Wild type		Y160F		K230M	
	Soln.	Crystal	Soln.	Crystal	Soln.	Crystal
	D-isocitrate to α-ketoglutarate (overall forward)					
k_{cat}(s^{-1})	76.2	38.3	0.311	0.276	0.850	0.78
K_m (mM)	0.011	2.8	0.0096	0.230	0.603	10.9
k_{cat}/K_m (s^{-1} mM^{-1})	6927		32.4	1.200	100.9	0.072
	D-isocitrate to oxalosuccinate					
k_{dehyd} (s^{-1})	789.0		0.311		238.0	
K_m (mM)	0.013		0.0096		0.673	
k/K_m (s^{-1} mM^{-1})	60692		32.4		354.0	
	Oxalosuccinate to α-KG					
k_{elim} (s^{-1})	20.6	28.3	36.2	33.8	<0.01	<0.01
K_m (mM)	0.22	5.2	0.22	6.10		
k/K_m (s^{-1} mM^{-1})	936	5.4	164.5	5.54		
	Oxalosuccinate to D-isocitrate					
k_{hyd} (s^{-1})	1.41	1.72	0.053	0.031	0.368	0.421
K_m (mM)	0.34	2.81	0.562	6.135	2.050	32.0
k/K_m (s^{-1} mM^{-1})	4.15	0.61	0.094	0.005	0.179	0.013
	Rate limits					
	Oxalosuccinate-NADPH		Isocitrate-$NADP^+$		Oxalosuccinate-NADPH	
	Soln.	Crystal	Soln.	Crystal	Soln.	Crystal
$t_{1/2}$ (ms)	9.1	9.3	2228	2511	815	889
Rate partition	>10	>10	$>10^3$	$>10^3$	$>10^2$	$>10^2$

* The rate partition is an estimate of the ratio of the individual forward rates leading into and out of the rate-limited enzyme complex. For the wild-type and K230M enzymes, this is the ratio of the initial burst kinetic rate over the steady-state rate; for Y160F it is conservatively estimated as the wild-type steady-state rate (which should reflect the slowest possible on rate for substrate binding) over the mutant's rate of dehydrogenation of the Michaelis complex. Bold type indicates effected rate-limit for each site-directed mutant.

and steady-state intermediate accumulation, it is necessary to determine: (i) the overall rate and binding constants in the crystal compared to values in solution, (ii) whether turnover occurs throughout the interior volume of the crystal or only at the enzyme molecules found at its surface, (iii) whether a given enzyme species is truly rate-limited at a single specific reaction step, allowing the homogeneous accumulation and observation of distinct intermediate states different from substrate and product, and (iv) the rate of diffusion and binding in the crystal. Our studies (Table 2 and Fig. 3), show that crystals of the mutant enzyme species may be saturated through the continuous presentation of substrate with a flow cell, and that a specific intermediate accumulates for each that may be observed crystallographically as described above. The crystallographic data described are consistent with kinetic studies on the enzyme.

The overall forward rate constants of the wild-type enzyme and both mutants has been measured in the crystal (Table 2). For both mutants, the maximum turnover rate was approximately 90 percent of maximal rate in solution, whereas the apparent binding constants were all about 20 times higher because of competition with sulfate for binding. The site-directed mutants both turn over at a rate less than 1 s^{-1} and form saturated, steady-state substrate complexes in the crystallographic flow cell. Calculations of the rate of production of product in these experiments, compared to the number of enzyme molecules in the crystals (determined by activity measurements and total protein determinations from dissolved crystals after kinetic measurements as described in Fig. 3), demonstrate that the enzyme is binding substrate and turning over throughout the body of the crystal rather than only at the surface.

The two catalytic steps after production of the initial ternary Michaelis complex are each freely reversible and separable from one another, with oxalosuccinate proposed to act as a substrate for the reverse hydrogenation reaction and for the forward elimination reaction. Therefore we can measure the rates not only of the overall forward and reverse rate constants, but also the location and magnitude of a rate change in the overall pathway of a mutagenized enzyme species relative to the wild-type catalyst. These studies indicate that the two site-directed mutants, Y160F and K230M, are amenable to steady-state Laue experiments. Each mutant displays an approximate wild-type rate constant for one half-reaction with oxalosuccinate as substrate, but a substantial rate decrease for the other half reaction, producing two different rate-limited intermediates.

The K230M mutant effects the dehydrogenation step at a slightly slower rate and is extremely slow to catalyze the elimination of the β carboxyl. The ratio of the rate of formation to the rate of degradation of oxalosuccinate, which forms the partition driving the accumulation of this intermediate is greater than 10^3, and the overall rate constant is 0.85 s^{-1}. Conversely, the Y160F mutant displays a wild-type rate of decarboxylation, but is slowed during the initial hydride transfer and formation of oxalosuccinate by more than 10^3, with an overall rate constant of 0.311 s^{-1}. In this case the rate-limited species is the initial ternary Michaelis complex, based on the slow rate of hydride transfer compared to the unchanged substrate binding constants and the on-rates. Thus, both mutants are very slow, and are severely rate-limited at two sequential intermediates within the overall reaction. The structures and ligand interactions of each enzyme mutant, both uncomplexed and bound with isocitrate, are isomorphous with the wild-type enzyme, indicating that the structural changes caused by these mutations are largely limited to the loss of specific chemical groups at these side chains (*16*). Each mutant appears to follow a catalytic mechanism unchanged from the wild-type enzyme, but slowed down at a single clearly identified reaction step resulting from the loss of a reactive group at the end of a side chain.

The reduction of $NADP^+$ to NADPH in the first reaction step provides a spectroscopic marker that may be used for the determination of substrate diffusion rates leading to accumulation of the rate-limited complex throughout the crystal. Single-crystal visible absorbance studies indicate that diffusion of sustained saturating concentrations of substrates throughout the crystal and the resulting formation of the steady-state complex takes approximately 10 to 15 seconds (Fig. 3). Direct spectroscopic measurement of the accumulation of reduced NADPH in the crystal also confirms the accumulation of different, and distinctive catalytic species in the active sites of the two enzyme mutants. As predicted by the kinetic rate studies summarized in Table 2, crystals of K230M show a broad absorbance peak that indicates the accumulation of a rate-limited complex containing reduced NADPH rather than $NADP^+$. Crystals of the tyrosine mutant Y160F, however, do not exhibit as substantial a color change even though they turn over at a rate comparable to that of K230M because the rate-limiting step is the production of NADPH.

Structural studies of catalytic intermediates by means of mutagenesis and Laue diffraction. Active site mutations together with Laue crystallography were used to observe two intermediates on the reaction pathway of isocitrate dehydrogenase. One of these intermediates is the long-postulated (but never observed) oxalosuccinate intermediate, the other is an intermediate that is formed just before hydride ion transfer. Both of the mutant enzymes studied are active and catalyze the overall reaction over 10^6 times more effectively than under non-enzymatic conditions. Nevertheless, the pathway is slowed at two key catalytic steps, thus allowing the accumulation of two in-

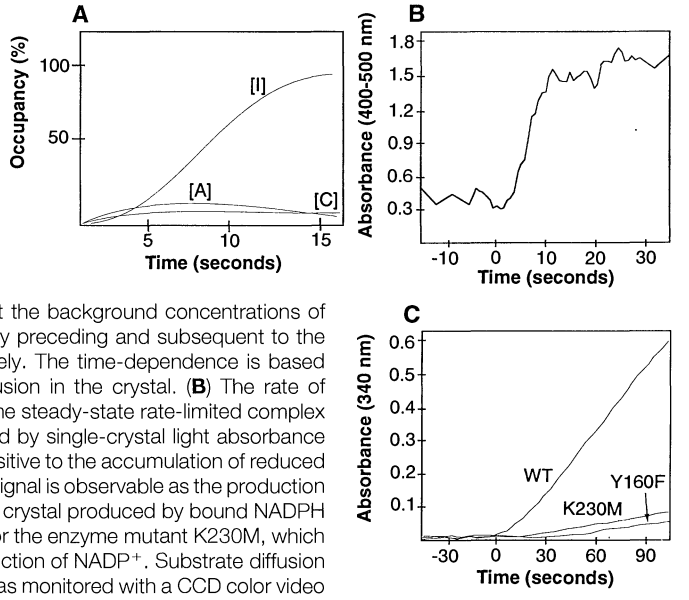

Fig. 3. Summary of rate studies in the crystal. Based on the individual rates shown in Table 2, the calculated concentration of the rate-limited intermediate species [I] for either mutant (expressed as the percentage of total active sites in the crystal) is greater than 95 percent at steady state. (**A**) and (**C**) represent the background concentrations of the catalytic species directly preceding and subsequent to the rate-limited step, respectively. The time-dependence is based on measured rates of diffusion in the crystal. (**B**) The rate of diffusion and formation of the steady-state rate-limited complex in the crystal was measured by single-crystal light absorbance spectroscopy, which is sensitive to the accumulation of reduced NADPH in the crystal. This signal is observable as the production of visible yellow color in the crystal produced by bound NADPH and is particularly intense for the enzyme mutant K230M, which is rate-limited after the reduction of $NADP^+$. Substrate diffusion and binding in the crystal was monitored with a CCD color video camera (Javelin). (C) Turnover rates and Michaelis binding constants were determined for both mutant enzyme species both in solution and in the crystal as described in Table 1. Varying concentrations of substrate (isocitrate), and a constant saturating concentration (100 mM) of $NADP^+$, and Mg^{+2} in artificial mother liquor (40 percent saturated ammonium sulfate at pH 7.5) were applied to the crystal in a flow cell at a rate of 2 ml/min. After saturation of the crystal, a reproducible linear rate of increase in the absorbance of the effluent at 350 nm was measured for each mutant (*26*).

termediates that otherwise never build up to an appreciable concentration. Because many wild-type enzyme catalysts have evolved to operate very efficiently, with turnover rates much faster than 1 s^{-1} and with few extreme energy barriers between sequential intermediates, such strategies are increasingly important for the application of time-resolved crystallography to the structure determination of important enzyme intermediates. This is because typical strategies for driving the synchronized accumulation of a specific intermediate during a single turnover event, such as flash-photolysis of a caged substrate molecule, are dependent on a finite rate of substrate binding and induced conformational changes after photolysis. That rate will often not be fast enough to synchronize accumulation of a specific intermediate throughout the crystal, particularly when there is no single predominant rate-limiting step. However, the techniques of site-directed mutagenesis and kinetic analysis provide an alternative strategy that allows for the accumulation and isolation of various catalytic intermediates for structure determination.

REFERENCES AND NOTES

1. J. Hajdu *et al.*, *Nature* **329**, 178 (1987).
2. I. Schlichting *et al.*, *ibid.* **345**, 309 (1990).
3. B. L. Stoddard, P. Koenigs, N. Porter, K. Petratos, G. A. Petsko, D. Ringe, *Proc. Natl. Acad. Sci. U.S.A.* **88**, 5503 (1991).
4. P. Singer, A. Smalas, R. P. Carty, W. F. Mangel, R. M. Sweet, *Science* **259**, 669 (1993).
5. V. Fulop *et al.*, *Structure* **2** (3), 201 (1994).
6. L. Johnson, *Protein Sci.* **1**, 1237 (1992).
7. G. A. Petsko, *Phil. Trans. R. Soc. (London)* **A340**, 323 (1992).
8. D. M. Blow *et al.*, *ibid.*, p. 311.
9. A. D. Cameron *et al.*, *Biochemistry* **32**, 13061 (1993).
10. N. C. J. Strynadka *et al.*, *Nature* **359**, 700 (1992).
11. A. J. Scheidig, *Acta Crystallogr. D* **50**, 512 (1994).
12. J. H. Hurley, A. M. Dean, J. L. Sohl, D. E. Koshland Jr., R. M. Stroud *Science* **249**, 1012 (1990).
13. J. H. Hurley, A. M. Dean, D. E. Koshland Jr., R. M. Stroud, *Biochemistry* **30**, 8671 (1991).
14. G. Plaut, in *The Enzymes*, P. D. Boyer *et al.*, Eds. (Academic Press, New York, ed. 2, 1963), pp. 112–129.
15. C. B. Grissom and W. W. Cleland, *Biochemistry* **27**, 2934 (1988).
16. M. Lee, O. Klein, J. Bolduc, D. Dyer, B. L. Stoddard, D. E. Koshland Jr., *Biochemistry* **34**, 378 (1995).
17. E. D. Getzoff *et al.*, *Nuclear Instrument. Methods Phys.* **B79**, 249 (1993).
18. A. T. Brünger, J. Kuriyan, M. Karplus, *Science* **235**, 458 (1987).
19. C. Walsh, *Enzymatic Reaction Mechanisms* (Freeman, New York, ed. 1, 1979), pp. 344–347.
20. M. F. Reid and C. A. Fewson, *Crit. Rev. Microbiol.* **20**, 13 (1994).
21. A. M. Dean and D. E. Koshland Jr., *Biochemistry* **132**, 9302 (1992).
22. B. L. Stoddard, A. M. Dean, D. E. Koshland Jr., *Biochemistry* **32**, 9310 (1992).
23. J. R. Helliwell *et al.*, *J. Appl. Crystallogr.* **22**, 483 (1989).
24. S. Ochoa, *J. Biol. Chem.* **174**, 115 (1948).
25. We have challenged and tested this method by conducting similar experiments using free enzyme ± NADP(H). The crystals were framed and digitized in each image with the software NIH-Image, and the signal was quantitated over time by integration and averaging of the total absorbance over the individual frames, so that we could monitor the time-dependent accumulation of reduced nicotinamide in the crystal as an increase in absorbance.
26. This experiment, which monitors total production of product over time by the crystal, was performed with a dead-end cuvette in a UV/VIS diode-array spectrophotometer (HP 8452) fed by the effluent from the crystal. Therefore, during this experiment the mother liquor volume and total product concentration in the cuvette were continuously increasing (Fig. 3), whereas the concentration of NADPH being released directly from the crystal shows a plateau at steady state. This led to the linear rate of increase in absorbance on formation of steady state. The experiment was conducted in this manner because of its high accuracy and precision in determining total product formation from a crystal. From the measured extinction coefficient of reduced NADPH in the mother liquor, the total product detected was converted to micromoles of product released from the crystal per second. The number of enzyme molecules in the crystals was measured (by dialyzing and dissolving the crystals and assaying maximal activity in solution relative to enzyme standards, followed by determination of total protein concentration by mass spectrophotometric analysis) and seen to agree with the expected value based on the dimension, specific volume, and density of the crystal. This value was used to calculate actual overall turnover rates in the crystal per enzyme molecule (0.28 and 0.85 s^{-1} per Y160F and K230M monomer, respectively). From these experiments it is clear that the entire volume of the enzyme crystal participates in binding and catalysis, rather than only the surface. Maximal rates of absorbance increases for all three enzyme species when 100 mM isocitrate is applied as shown in Fig. 3C.

27. Supported by NIH grant GM49857 (B.L.S.) and by NSF grant 04200 (D.E.K.). We thank M. Soltis and P. Phizackerly of SSRL for advice and assistance, J. Bolduc, D. Dyer, and B. Scott contributed equally to this research project. The coordinates have been deposited in the Protein Data Bank (Code Numbers 1IDC, 1IDD, 1IDE, and 1IDF).

22 December 1994; accepted 17 April 1995